metals

MDPI

Article

The Effect of P on the Microstructure and Melting Temperature of Fe_2SiO_4 in Silicon-Containing Steels Investigated by In Situ Observation

Qing Yuan, Guang Xu *, Mingxing Zhou, Bei He and Haijiang Hu

The State Key Laboratory of Refractories and Metallurgy, Hubei Collaborative Innovation Center for Advanced Steels, Wuhan University of Science and Technology, 947 Heping Avenue, Qingshan District, Wuhan 430081, China; 15994235997@163.com (Q.Y.); kdmingxing@163.com (M.Z.); 15071412662@163.com (B.H.); hhjsunny@sina.com (H.H.)

* Correspondence: xuguang@wust.edu.cn; Tel.: +86-27-6886-2813

Academic Editor: Filippo Berto

Received: 28 November 2016; Accepted: 24 January 2017; Published: 27 January 2017

Abstract: In this study, two silicon-containing steels with different P contents were used, and reheating tests were conducted in an industrial furnace in a hot strip plant. The effect of P on the microstructure and melting temperature of Fe_2SiO_4 in silicon-containing steels was investigated using a backscattered electron (BSE) detector and energy-dispersive spectroscopy (EDS). The melting process of Fe_2SiO_4 was also observed in situ for the two steels with different P contents. The results show that the addition of P could lower the melting point of the eutectic compound Fe_2SiO_4/FeO, which is helpful for descaling the oxide scale. The melting point decreases with the increasing P content, and the melting point of Fe_2SiO_4/FeO can reduce up to 954.2 °C when the content of P reaches 0.115 wt %. Furthermore, P-compounds form in the dispersive particles located in the iron matrix near the interface between the matrix and inner oxide scale when the P content is relatively high. In addition, a method of in situ observation was proposed to study the effect of P on the melting point of Fe_2SiO_4/FeO in silicon-containing steel. The results are of more practical significance for the descaling of oxide scale in silicon-containing steel.

Keywords: in situ observation; Fe_2SiO_4; $Fe_3(PO_4)_2$; melting temperature; dispersive particles

1. Introduction

The eutectic compound Fe_2SiO_4/FeO is the main inducement of red scale in silicon-containing steel. In general, the formation of the red scale is related not only to the content of Fe_2SiO_4, but also to its morphology and distribution. The formation mechanism of red scale has been reported in several studies [1–8]. Silicon reacts with oxygen diffusing into steel and precipitates as SiO_2, which combines with FeO and then forms a separate phase called fayalite (Fe_2SiO_4). The theoretical melting point of Fe_2SiO_4/FeO is approximately 1173 °C and liquid Fe_2SiO_4 irregularly penetrates into FeO and the matrix. It is difficult to completely wipe off the FeO layer after descaling due to the very high strength of the eutectic compound Fe_2SiO_4/FeO. Following the cooling process, the remaining FeO scale is oxidized into red Fe_2O_3.

To eliminate the red scale defect, many studies on Fe_2SiO_4 of silicon-containing steels have been conducted. Suarez et al. [9] reported that the amount of Fe_2SiO_4 increases with the silicon content and the liquid Fe_2SiO_4/FeO is distributed in the net-like form between the iron matrix and the inner oxide scale when the temperature is higher than the melting temperature of Fe_2SiO_4/FeO, resulting in more red scale. Mouayd et al. [10] reported that the penetrative depth of the eutectic FeO/Fe_2SiO_4 in the scale increases with the silicon content. In the present authors' previous study [11] on the relationship

between silicon content and morphology of Fe_2SiO_4, it was shown that Fe_2SiO_4 appears in a net-like form in the innermost layer of oxide scale close to the iron matrix when the silicon content is 1.21 wt %. However, no obvious net-like Fe_2SiO_4 is observed when the silicon content is less than 0.25 wt %. In addition, the effects of chemical compositions on the scale were investigated by Kizu et al. [12]. They found that the blistering of the scale was promoted by increasing C, Mn and P contents and suppressed by increasing the S content at any temperature. Furthermore, Yu et al. [13] took the chemical compositions into account while investigating the tertiary scale characteristics of hot rolled strips. They pointed out that P can be enriched at the interface between the substrate and tertiary scale, which is beneficial to decrease the adhesion of the tertiary scale. However, Si enrichment at the interface between the substrate and tertiary scale increases the adhesion.

It is noteworthy that Fukagawa et al. [14] suggested a new method to decrease the red scale from the perspective of the effect of chemical compositions on the Fe_2SiO_4. They demonstrated that the addition of P lowers the binary eutectic temperature of FeO/Fe_2SiO_4 oxides (1167 °C, close to the theoretical melting point temperature of FeO/Fe_2SiO_4) formed during slab soaking, because the sarcopside ($Fe_3(PO_4)_2$) crystallizes in oxide scale when the content of P reaches a certain value. This leads to the formation of a ternary eutectic $FeO/Fe_2SiO_4/Fe_3(PO_4)_2$ having a low melting point of 890 °C. The appearance of $Fe_3(PO_4)_2$ lowers the binary eutectic temperature of FeO/Fe_2SiO_4. Therefore, the liquid eutectic compound in the scale/steel interface during the descaling improves the hydraulic-descaling-ability. However, in their studies, the measurement of melting points of FeO/Fe_2SiO_4 and other analyses on the oxide scale were based on differential scanning calorimetry (DSC) on the different reagent powders of Fe, Fe_3O_4, SiO_2 and P_2O_5. Meanwhile, the research about the effect of P on the oxide scale is scarce. Therefore, the present study focused on the effect of P on the microstructure and melting temperature of Fe_2SiO_4. First, two low-carbon steels with different P contents were used and heated in an industrial furnace. The chemical constitutions and experimental conditions of oxide scale conformed to the industrial scenario. Secondly, an in situ observation method was used to determine the melting point of FeO/Fe_2SiO_4; the melting process of FeO/Fe_2SiO_4 was completely recorded. The results are of more practical significance and provide a useful reference for the control of red scale defect in silicon-containing steels.

2. Materials and Methods

2.1. Industrial Oxidation Experiment

Tested materials were taken from two silicon-containing steels commercially produced in a hot strip plant (Baosteel, Shanghai, China). The chemical compositions of the two steels with different P contents were determined by a carbon sulfur analyzer (CS-8800) and infrared spectrometer (IS50) and are presented in Table 1. The samples were polished to remove the scale before heating in the furnace. The industrial reheating procedure is presented in Figure 1a. The samples were heated to 1260 °C by a segment heating route and held for 40 min, followed by air cooling to ambient temperature. The heating atmosphere in the furnace contained approximately 2% oxygen, 13% carbon dioxide, 11% water vapor and 74% nitrogen (vol %). After the oxidation experiment, three or more specimens of each steel were cut using a wire-electrode cutting device (HFang, Taizhou, China) whose flow velocity of lubricant was controlled in a relatively lower value for keeping the integrity of oxide scale. Moreover, a cold mounting method was used in the preparation of the samples for microscopic observation. The conventional hot mounting method was not utilized in the present study due to the strong compressive stress during the mounting process which is harmful for the protection of oxide scale. The cold mounting material is composed of 60% acrylic powder and 40% liquid hardener. The cross-sections of mounted samples were ground and polished. Subsequently, the microstructures were observed using a backscattered electron (BSE) detector on a Nova 400 Nano scanning electron microscope (SEM) (Hillsboro, OR, USA), operated at an accelerating voltage of 20 kV. Energy-dispersive spectroscopy (EDS) was applied to analyze the compositions of the oxide scale.

Two acquisition techniques, including point analysis and selected area elemental mapping, were employed. To obtain a better intensity of spectral lines, the acceleration voltage was selected to be a relatively low value as 18 kV. Appropriate long acquisition time was used to ensure sufficient acquisition counts (cts). For example, the acquisition time and counts are 155 s and 272,926, respectively, according to the following result of selected-area elemental mapping.

Table 1. The chemical compositions of the tested steels (wt %).

Steels	C	Si	Mn	P	S	Ni	Als	Ti	Fe
SiP-1	0.069	1.310	1.240	0.020	0.001	0.012	0.037	<0.004	Bal.
SiP-2	0.070	1.300	1.260	0.115	0.002	0.010	0.035	<0.004	Bal.

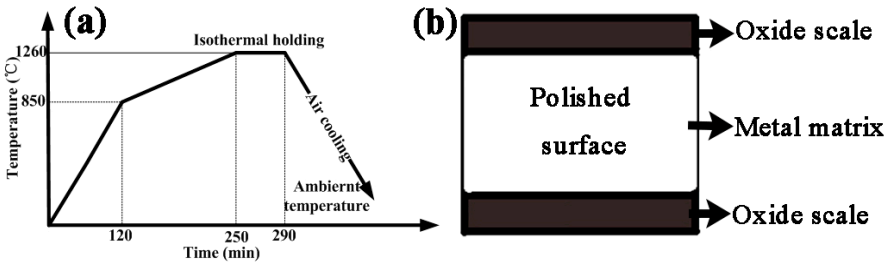

Figure 1. (**a**) The industrial heating procedure; (**b**) The schematic diagram of a sample for in situ observation.

2.2. In Situ Observation of the Melting Process of Fe_2SiO_4

The melting process of Fe_2SiO_4 was observed in situ using a VL2000DX laser scanning confocal microscope (LSCM) (Lasertec, Yokohama, Japan). The samples for in situ observations were prepared after the industrial oxidation experiments. The specimens were machined into a cube-shaped structure with dimensions of 4 mm × 4 mm × 4 mm. To maintain a level observation surface, the cross-section of the oxide scale and its opposite sides of the samples were conventionally polished. The polished surfaces were perpendicular to the observation direction. The Fe_2SiO_4 layer still adhered to the polished sample (Figure 1b). The specimen chamber was initially evacuated to 6×10^{-3} Pa before heating, and argon was used to protect the specimens from surface oxidation. The specimens were heated at a fast heating rate of 5 °C·s^{-1} to 800 °C. Furthermore, to clearly observe the melting process of Fe_2SiO_4, the specimens were then heated at a slow heating rate of 0.15 °C·s^{-1} to 1200 °C followed by 0.2 °C·s^{-1} to 1260 °C. Finally, the specimens were maintained at 1260 °C for 2 min and then cooled to an ambient temperature at 2 °C·s^{-1}. The LSCM images were continuously recorded at 15 frames·s^{-1} at a magnification of 500× during the whole heating treatment. A video showing the melting process of Fe_2SiO_4 was simultaneously recorded.

3. Results and Discussion

3.1. Microstructural Characterization of the Oxide Scale

Figure 2 shows the SEM images of the oxide scale in the two tested steels obtained with the backscattered electron (BSE) detector. As depicted in previous studies [15,16], the oxide scale mainly consists of three different layers, i.e., the upper layer Fe_2O_3, middle layer FeO + Fe_3O_4, and inner layer FeO/Fe_2SiO_4. The outer layers of Fe_2O_3 and FeO + Fe_3O_4 are brittle and easy to wipe off, but the inner layer of FeO/Fe_2SiO_4 strongly adheres to the metal matrix and is retained completely. The dark phase close to the scale–metal interface is a mixture of Fe_2SiO_4 and FeO. The red area in thumbnails located at the bottom left of Figure 2a,b is obtained by an image-processing software, Image-Pro plus 6.0 (Media Cybernetics, Rockville, MD, USA). Initially, the total area of Fe_2SiO_4 in the inner layers is isolated and measured by the auto-discernment function of color aberration in the software. Subsequently,

to obtain the areas of Fe_2SiO_4 in unit widths, the total areas are divided by the width of the measured images [11]. The red area represents the distributions of solid Fe_2SiO_4 and the measured area can represent the amount of Fe_2SiO_4. Figure 2c shows the contents and penetration depths of Fe_2SiO_4 in the two specimens. Only the penetration depth of Fe_2SiO_4 into the FeO layer is considered because the formation mechanism of red scale is mainly related with the "anchor effect" between the upper FeO and lower Fe_2SiO_4. The result indicates that the contents of Fe_2SiO_4 in both the two tested steels have no significant difference. In addition, the penetration depths of Fe_2SiO_4 are almost the same. This is because the content and penetration depth of Fe_2SiO_4 are related to the silicon content [17–21], and the silicon contents in two tested steels are basically the same. Furthermore, the reasons for the net-like distribution of Fe_2SiO_4 can be explained by compressive stress at the oxide layer/metal interface [22]. The compressive stress at the oxide layer/metal interface is larger than that at the outer position when the Pilling–Bedworth Ratio (PBR) is more than 1 [23], resulting in the pressure differences between the interface and outside oxidation layer. The pressure difference always exists along with the displacement of the oxidation reaction interface [11,16,22]. The pressure difference in the liquefied Fe_2SiO_4 phase at a temperature higher than the melting point of Fe_2SiO_4 forces a part of Fe_2SiO_4 to permeate into the inner scale. The liquid Fe_2SiO_4 phase distributes along the FeO grain boundaries and the net-like Fe_2SiO_4 phase forms after its solidification. Moreover, the net-like Fe_2SiO_4 phase may also be related to the possibility of Si diffusion through FeO grain boundaries and possible oxidation there.

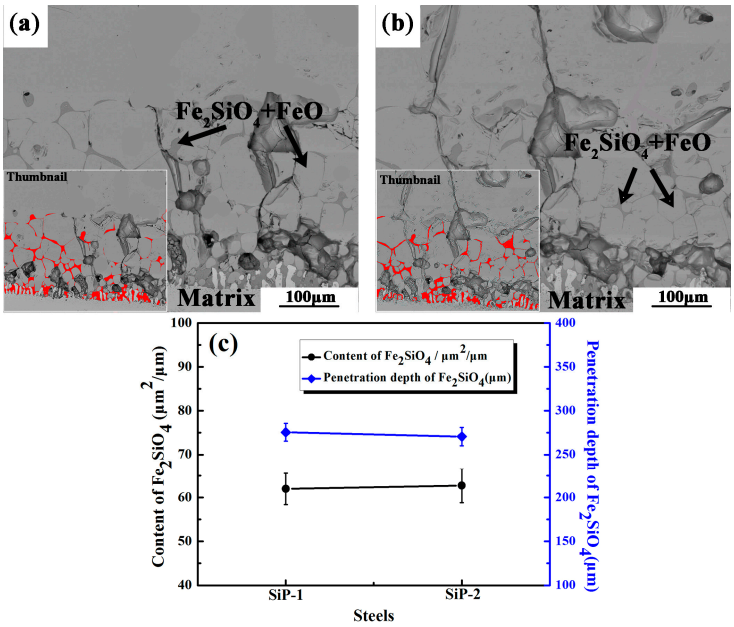

Figure 2. SEM images of the oxide scale obtained with the backscattered electron (BSE) detector. (**a**) SiP-1; (**b**) SiP-2; (**c**) The contents and penetration depths of Fe_2SiO_4 in the two specimens.

3.2. Distribution of Chemical Elements in the Fe_2SiO_4 Phase

The distributions of chemical elements in the Fe_2SiO_4 phase are illustrated in Figure 3. To observe the phase of spectrum such as the area of spectrum 1 in Figure 3a with greater clarity, the magnification of Figure 3b is larger than that of Figure 3a. Figure 3a shows that the oxygen content gradually decreases from the upper layer (spectrum 2) to the inner layer (spectrum 1). The oxygen content is relatively higher than the standard of iron oxide, probably because the oxygen sensitivity of the applied method (EDS) is not very good, resulting in a variable oxygen content. However, the Mn content increases from the outside to inside of the scale as a result of Mn diffusion from the metal to the oxide [24]. In addition, the contents of P in Fe_2SiO_4 of steel SiP-1 are much smaller, because of

less P content in the steel SiP-1 (Table 1). The P content changes within a small range when it is quite small due to the limited sensitivity of the detectors in the EDS units. The maximum values for spectra 1 and 2 in Figure 3a are 0.02 and 0.03 (at %), respectively, demonstrating that the concentration of P element is very small. The atomic percentage of Fe:Si:O in spectra 1 and 2 (Figure 3a) is calculated to be approximately 2:1:4. Therefore, the dark gray district (net-like area) in Figure 3a is mainly the Fe_2SiO_4 phase and no $Fe_3(PO_4)_2$ phase is detected. On the other hand, the elemental distribution of spectrum 2 in Figure 3b is similar to that of Figure 3a. There is more P element in the spectrum 1, seen as a bright gray district in Figure 3b. The atomic percentage of Fe:P:O in spectrum 1 is calculated to be approximately 2.5:2.0:7.0, which is near to the standard atomic percentage of the $Fe_3(PO_4)_2$ phase. According to previous studies [12–14], P only exists as the $Fe_3(PO_4)_2$ phase which has an orthorhombic system as the Fe_2SiO_4 phase and aggregates at the interface between the scale and substrate. Therefore, it can be inferred that the phase in spectrum 1 of Figure 3b is mainly $Fe_3(PO_4)_2$. Therefore, there is only the Fe_2SiO_4 phase in the sample with less P content (Figure 3a), whereas there are two phases, Fe_2SiO_4 and $Fe_3(PO_4)_2$, in the sample with high P content (Figure 3b).

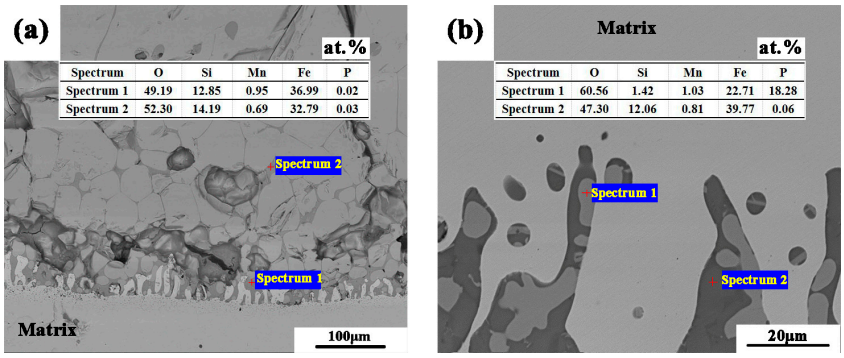

Figure 3. The distributions of chemical elements in the Fe_2SiO_4 phase (**a**): SiP-1; (**b**): SiP-2.

In addition, there were many dispersive particles located in the iron matrix near the interface between the matrix and inner oxide scale. In previous studies [5,6,11], these dispersive particles have been proven to be silicon dioxide in steels containing less P content. Figure 4 shows the results of selected-area elemental mapping on the dispersive particles located in the steel matrix near the interface between the iron matrix and inner oxide scale for steel SiP-2 containing 0.115 wt % P. P element can also be detected in these particles. Figure 5 gives the chemical compositions of the dispersive particles obtained by the point analysis method of EDS. It clarifies that not only silicon dioxide exists in these dispersive particles, but also P-compounds can be found when steel contains a higher P content.

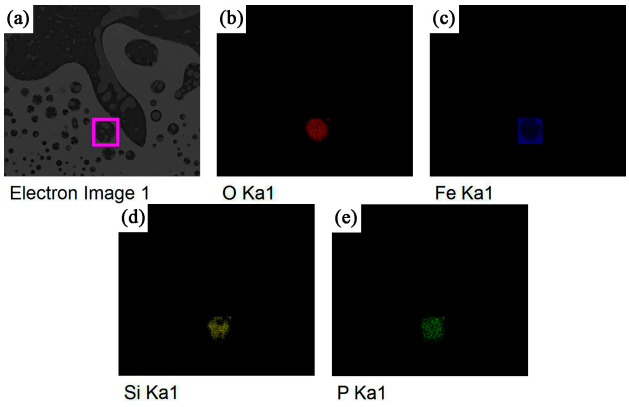

Figure 4. (**a**–**e**) The selected-area elemental mapping on dispersive particles located near the interface between the matrix and inner oxide scale.

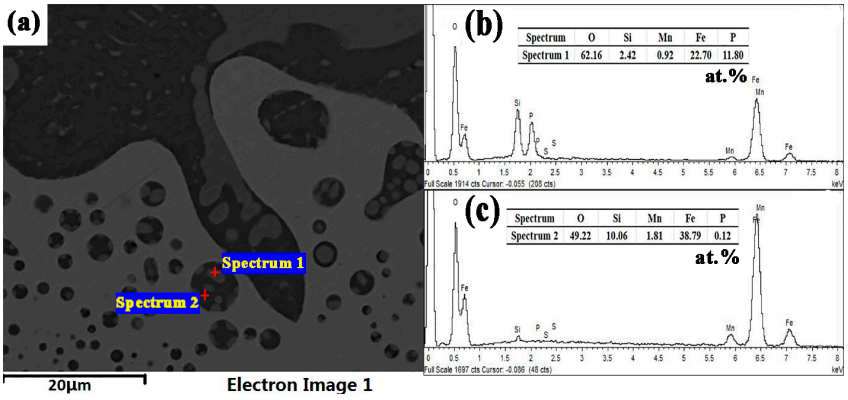

Figure 5. The chemical composition of the dispersive particles obtained by the point analysis method of EDS (**a**) the morphology of dispersive particles; (**b**) the elemental constitution of spectrum 1; (**c**) the elemental constitution of spectrum 2.

3.3. In Situ Observation of the Melting Process of Fe_2SiO_4

Figure 6 presents micrographs showing results from in situ observations of the melting process of Fe_2SiO_4 for steel SiP-1 (1.31 wt % Si; 0.020 wt % P). Figure 6a shows the morphology of oxide scale before melting. Fe_2SiO_4 is distributed in the net-like form. Figure 6b illustrates that the Fe_2SiO_4 phase begins to melt at 1170.6 °C, which is close to the theoretical melting temperature of Fe_2SiO_4 (1173 °C). It demonstrates that the melting point of Fe_2SiO_4 is close to the theoretical melting temperature when P content is relatively low. In earlier studies [1,3,5,9,25], the melting temperature of Fe_2SiO_4 was approximately 1173 °C because the P content was less than 0.051 wt %. Figure 6c shows the morphology of liquid Fe_2SiO_4 during melting; the FeO phase is still in the solid state due to its higher melting point (1370 °C). The end of the melting process of Fe_2SiO_4 is presented in Figure 6d. The time taken for the entire melting process of Fe_2SiO_4 is approximately 136.4 s.

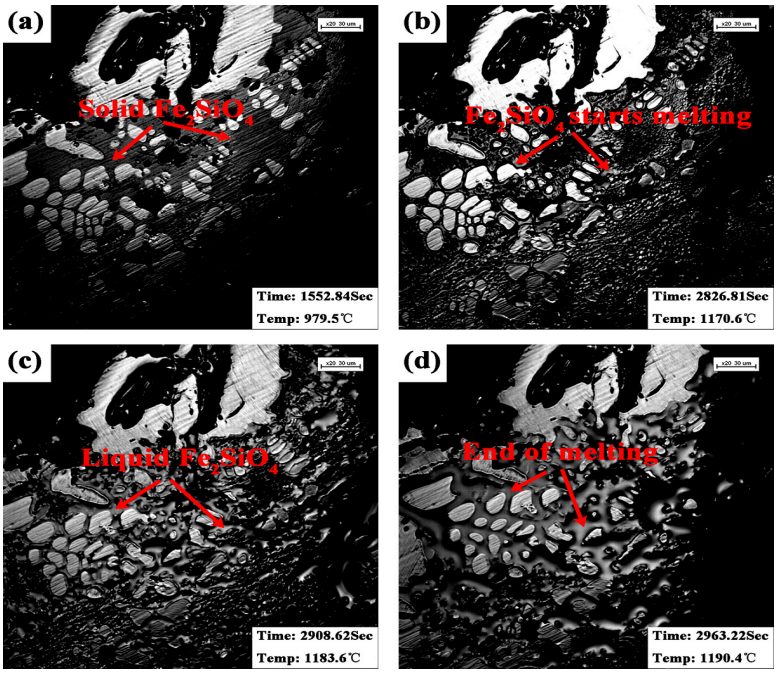

Figure 6. Micrographs showing results from in situ observations of the melting process of Fe_2SiO_4 for steel SiP-1 (**a**) before melting; (**b**) at the start of melting; (**c**) during melting; (**d**) at the end of melting.

The micrographs showing results from in situ observations of the melting process of Fe_2SiO_4 for steel SiP-2 (1.30 wt % Si; 0.115 wt % P) are given in Figure 7. Figure 7a shows the morphology of oxide scale before melting, and Figure 7b shows that the Fe_2SiO_4 phase begins to melt at 954.2 °C. The melting point of Fe_2SiO_4/FeO of steel SiP-2 is obviously lower than that of steel SiP-1 as well as the theoretical melting temperature of Fe_2SiO_4/FeO (1173 °C). It demonstrates that the melting point of Fe_2SiO_4/FeO decreases with the increasing P content. Therefore, this is an effective and practical way to decrease the Fe_2SiO_4 melting temperature with the addition of P element. By this way, the Fe_2SiO_4 phase is in a liquid state and can be removed easily when the descaling temperature is higher than the melting temperature of Fe_2SiO_4. Figure 7c illustrates the morphology of liquid Fe_2SiO_4 during melting. The end of the melting process of Fe_2SiO_4 is shown in Figure 7d. The time taken for the entire melting process of Fe_2SiO_4 is approximately 1458.5 s.

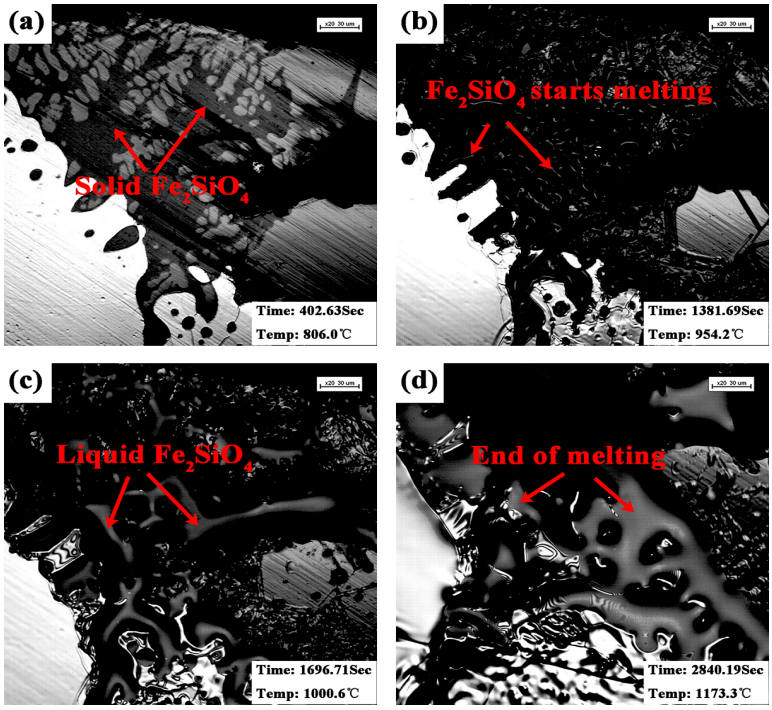

Figure 7. Micrographs showing results from in situ observations of the melting process of Fe_2SiO_4 for steel SiP-2 (**a**) before melting; (**b**) at the start of melting; (**c**) during melting; (**d**) at the end of melting.

Figure 8 shows the image of the FeO-SiO_2-P_2O_5 ternary eutectic system, which is reported by Fukagawa et al. [14]. This FeO-SiO_2-P_2O_5 ternary eutectic system is a regional image of the whole FeO-SiO_2-P_2O_5 ternary eutectic system which is obtained by the combination of three different binary eutectic systems. There are three temperature scales in the whole ternary eutectic system. For easier understanding of the ternary eutectic system, a regional image without temperature scales is used in the present study. Moreover, the three characteristic temperatures are given in order to show the relationship between the temperature and different phases. There are three different stages during the cooling process. First, the FeO phase crystallizes when the temperature is relatively high (point M_I (~1200 °C)). Then, the Fe_2SiO_4 phase starts crystallizing when the temperature decreases to point E_{II} (binary eutectic point (~954–1173 °C)). At last, the $Fe_3(PO_4)_2$ phase crystallizes when the temperature decreases to the point E_{III} (ternary eutectic (~890 °C)). Therefore, it can be concluded that the existence of $Fe_3(PO_4)_2$ phase can lower the binary eutectic point of compound Fe_2SiO_4/FeO. The results of this study also demonstrate that the addition of P could lower the melting point of the eutectic compound Fe_2SiO_4/FeO (Steel SiP-2), and a ternary eutectic compound $Fe_3(PO_4)_2$/Fe_2SiO_4/FeO forms upon the Fe_2SiO_4 phase area. It is easy to wipe off the red scale when the descaling temperature is higher than

the melting point of Fe_2SiO_4/FeO. The melting point of the eutectic compound Fe_2SiO_4/FeO decreases with the increasing P content, and it could reduce to 954.2 °C when the P content is 0.115 wt %. In addition, the $Fe_3(PO_4)_2$ phase is detected in the net-like Fe_2SiO_4 area, and P-compounds are in the dispersive particles located in the iron matrix near the interface between the matrix and inner oxide scale. Furthermore, the silicon-containing steels in the present study are commercially produced and their oxide scale is formed during the reheating process in the industrial production. Therefore, the results represent oxidation behavior of steel and oxide microstructures in actual production and can provide some valuable reference from the viewpoint of industrial application.

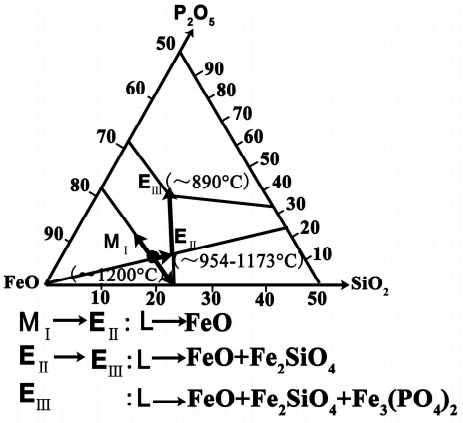

Figure 8. FeO-SiO_2-P_2O_5 ternary eutectic system.

4. Conclusions

In this study, two silicon-containing steels with different P contents were tested. High temperature oxidation tests were conducted in an industrial furnace in a hot strip plant. The effect of P on the microstructure and melting temperature of Fe_2SiO_4 in the two silicon-containing steel were investigated using a backscattered electron (BSE) detector on a Nova 400 Nano scanning electron microscope (SEM) and energy-dispersive spectroscopy (EDS). In situ observations of the melting process of Fe_2SiO_4 were conducted. The results indicate that the $Fe_3(PO_4)_2$ phase forms mainly at the interface between the iron matrix and inner oxide layer with the addition of P which could lower the melting point of the eutectic compound Fe_2SiO_4/FeO and the melting point of Fe_2SiO_4/FeO decreases with the increasing P content. The melting point of Fe_2SiO_4/FeO could reduce to 954.2 °C when the content of P is 0.115 wt %. In addition, when the P content is relatively high, P-compounds are formed in the dispersive particles located in the iron matrix near the interface between the matrix and inner oxide scale. Furthermore, the effect of P on the microstructure and melting temperature of Fe_2SiO_4/FeO in both the silicon-containing steels was investigated by in situ observation. This method may offer new insights for the research on metal oxidation and other fields of corrosion science.

Acknowledgments: The authors gratefully acknowledge the financial support from the National Natural Science Foundation of China (NSFC) (No. 51274154), the State Key Laboratory of Development and Application Technology of Automotive Steels (Baosteel Group).

Author Contributions: Guang Xu, supervisor, conceived and designed the experiments; Qing Yuan, doctoral student, conducted experiments, analyzed the data and wrote the paper; Mingxing Zhou, doctoral students, conducted experiments; Bei He, master students, conducted experiments; Haijiang Hu, doctoral students, conducted experiments.

Conflicts of Interest: The authors declare no conflict of interest.

References

1. Okada, H.; Fukagawa, T.; Ishihara, H. Prevention of red scale formation during hot rolling of steels. *ISIJ Int.* **1995**, *35*, 886–891. [CrossRef]

2. Okada, H.; Fukagawa, T.; Ishihara, H.; Okamoto, A.; Azuma, M.; Matsuda, Y. Effects of hot-rolling and descaling condition on red scale defects formation. *ISIJ Int.* **1994**, *80*, 849–854.
3. Fukagawa, T.; Okada, H.; Maeharara, Y. Mechanical of red scale defect formation in Si-added hot-rolled steels. *ISIJ Int.* **1994**, *11*, 906–911. [CrossRef]
4. Fukagawa, T.; Okada, H.; Maehara, Y.; Fujikawa, H. Effect of small amount of Ni on Hydraulic-descaling-ability in Si-added Hot-rolled Steel Sheets. *ISIJ Int.* **1996**, *82*, 63–68.
5. Liu, X.J.; Cao, G.M.; He, Y.Q.; Jia, T.; Liu, Z.Y. Effect of temperature on scale morphology of Fe-1.5Si alloy. *J. Iron Steel Res. Int.* **2013**, *20*, 73–78. [CrossRef]
6. Yang, Y.L.; Yang, C.H.; Lin, S.N.; Chen, C.H.; Tsai, W.T. Effects of Si and its content on the scale formation on hot-rolled steel strips. *Mater. Chem. Phys.* **2008**, *112*, 566–571. [CrossRef]
7. Cao, G.M.; Liu, X.J.; Sun, B.; Liu, Z.Y. Morphology of oxide scale and oxidation kinetics of low carbon steel. *J. Iron Steel Res. Int.* **2014**, *21*, 335–341. [CrossRef]
8. Zhou, M.X.; Xu, G.; Hu, H.J.; Yuan, Q.; Tian, J.Y. The morphologies of different types of Fe_2SiO_4–FeO in Si-containing steel. *Metals.* **2017**, *7*, 8–15. [CrossRef]
9. Suarez, L.; Schneider, J.; Houbaert, Y. High-temperature oxidation of Fe-Si alloys in the temperature range 900–1250 °C. In *Defect and Diffusion Forum*; Trans Tech Publications: Zurich, Switzerland, 2008; pp. 661–666.
10. Mouayd, A.A.; Koltsov, E.; Sutter, B.; Tribollet, B. Effect of silicon content in steel and oxidation temperature on scale growth and morphology. *Mater. Chem. Phys.* **2014**, *143*, 996–1004. [CrossRef]
11. Yuan, Q.; Xu, G.; Zhou, M.X.; He, B. The effect of the Si content on the morphology and amount of Fe_2SiO_4 in low carbon steels. *Metals* **2016**, *6*, 94–102. [CrossRef]
12. Taro, K.; Yasunobu, N.; Toru, I.; Yoshihiro, H. Effects of chemical composition and oxidation temperature on the adhesion of scale in plain carbon steels. *ISIJ Int.* **2001**, *41*, 1494–1501.
13. Yu, Y.; Wang, C.; Wang, L.; Chen, J.; Hui, Y.J.; Sun, C.K. Combination effect of Si and P on tertiary scale characteristic of hot rolled strip. *J. Iron Steel Res. Int.* **2015**, *22*, 232–237. [CrossRef]
14. Fukagawa, T.; Okada, H.; Fujikawa, H. Effect of P on hydraulic-descaling-ability in Si-added hot-rolled steel sheets. *Steels* **1997**, *83*, 305–311. (In Japanese)
15. Yuan, Q.; Xu, G.; Zhou, M.X.; He, B. New insights into the effects of silicon content on the oxidation process in silicon-containing steels. *Int. J. Miner. Metall. Mater.* **2016**, *23*, 1–8. [CrossRef]
16. He, B.; Xu, G.; Zhou, M.X.; Yuan, Q. Effect of oxidation temperature on the oxidation process of silicon-containing steel. *Metals* **2016**, *6*, 137–145. [CrossRef]
17. Kusabiraki, K.; Watanabe, R.; Ikehata, T. High-temperature oxidation behavior and scale morphology of Si-containing steels. *ISIJ Int.* **2007**, *9*, 1329–1334. [CrossRef]
18. Suarez, L.; Schneider, J.; Houbaert, Y. *Effect of Si on high-temperature oxidation of steel during hot rolling In Defect and Diffusion Forum*; Trans Tech Publications: Zurich, Switzerland, 2008; pp. 655–660.
19. Chen, R.Y.; Yuen, W.Y.D. Review of the high-temperature oxidation of iron and carbon steels in air or oxygen. *Oxid. Met.* **2003**, *59*, 433–468. [CrossRef]
20. Taniguchi, S.; Yamamoto, K.; Megumi, D.; Shibata, T. Characteristics of scale/substrate interface area of Si-containing low-carbon steels at high temperatures. *Mater. Sci. Eng. A* **2001**, *1*, 250–257. [CrossRef]
21. Li, S.J.; Liu, Y.B.; Zhang, W.; Sun, Q.S.; Wang, L.P. Effects of silicon on spring steel oxidation rate under 2% residual oxygen atmosphere. *J. Iron Steel Res. Int.* **2015**, *5*, 55–60. (In Chinese)
22. Garnaud, G.; Rapp, R.A. Thickness of the oxide layers formed during the oxidation of iron. *Oxid. Met.* **1977**, *11*, 193–198. [CrossRef]
23. Staettle, R.W.; Fontana, M.G. *Advances in Corrosion Science and Technology*; Springer-Verlag: New York, NY, USA, 1974; pp. 239–356.
24. Zhang, Y.S.; Rapp, R.A. Solubilities of CeO_2, HfO_2 and Y_2O_3 in Fused Na_2SO_4-30 mol% $NaVO_3$ and CeO_2 in Pure Na_2SO_4 at 900 °C. *Corrosion* **1987**, *43*, 348–352. [CrossRef]
25. Asai, T.; Soshiroda, T.; MiyaharaI, M. Influence of Ni impurity in steel on the removability of primary scale in hydraulic descaling. *ISIJ Int.* **1997**, *37*, 272–277. [CrossRef]